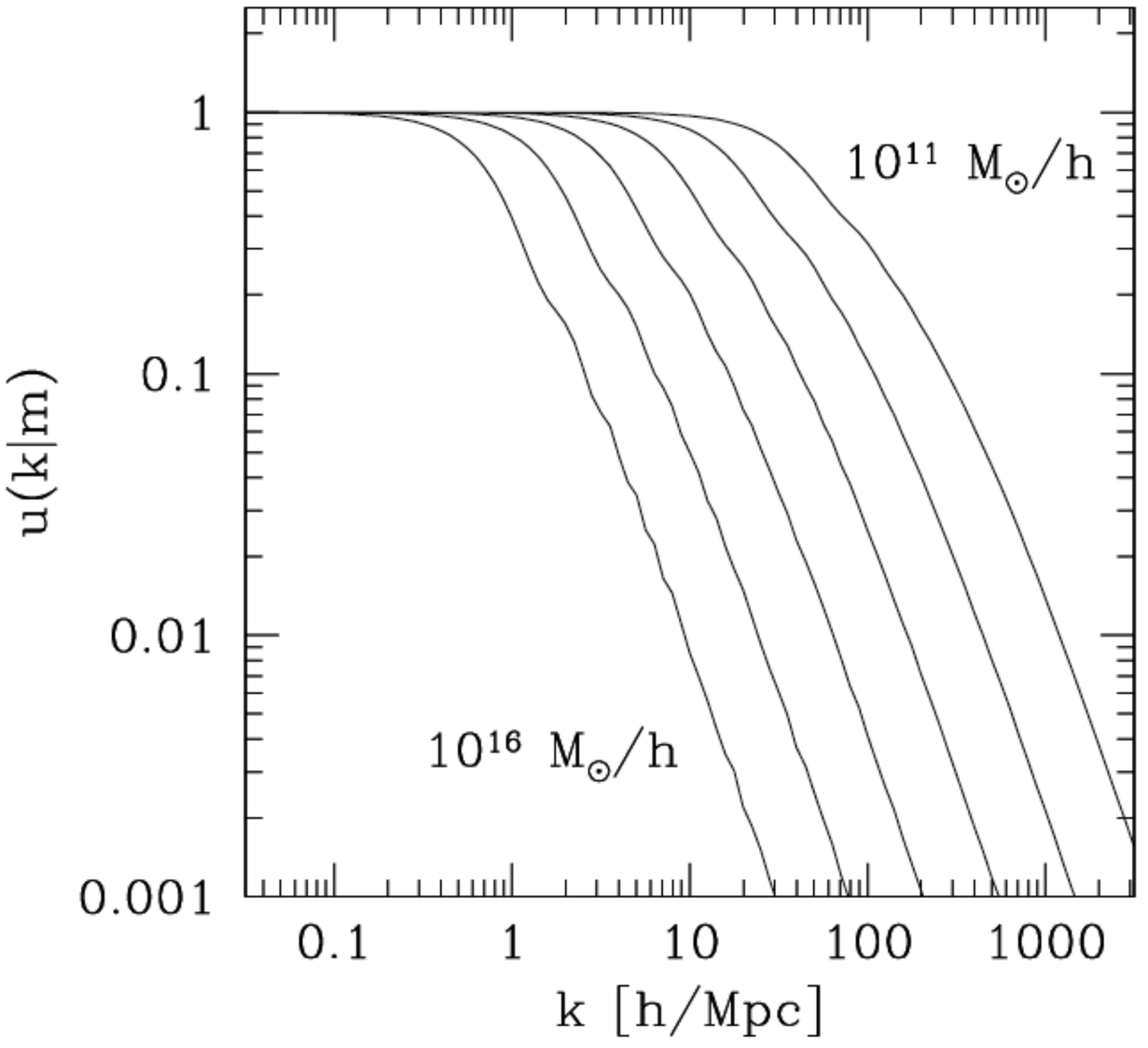
1
0.1
0.01
0.001
u(k|m)
10^{11} $M_\odot$/h
10^{16} $M_\odot$/h
0.1
1
10
100
1000
k [h/Mpc]

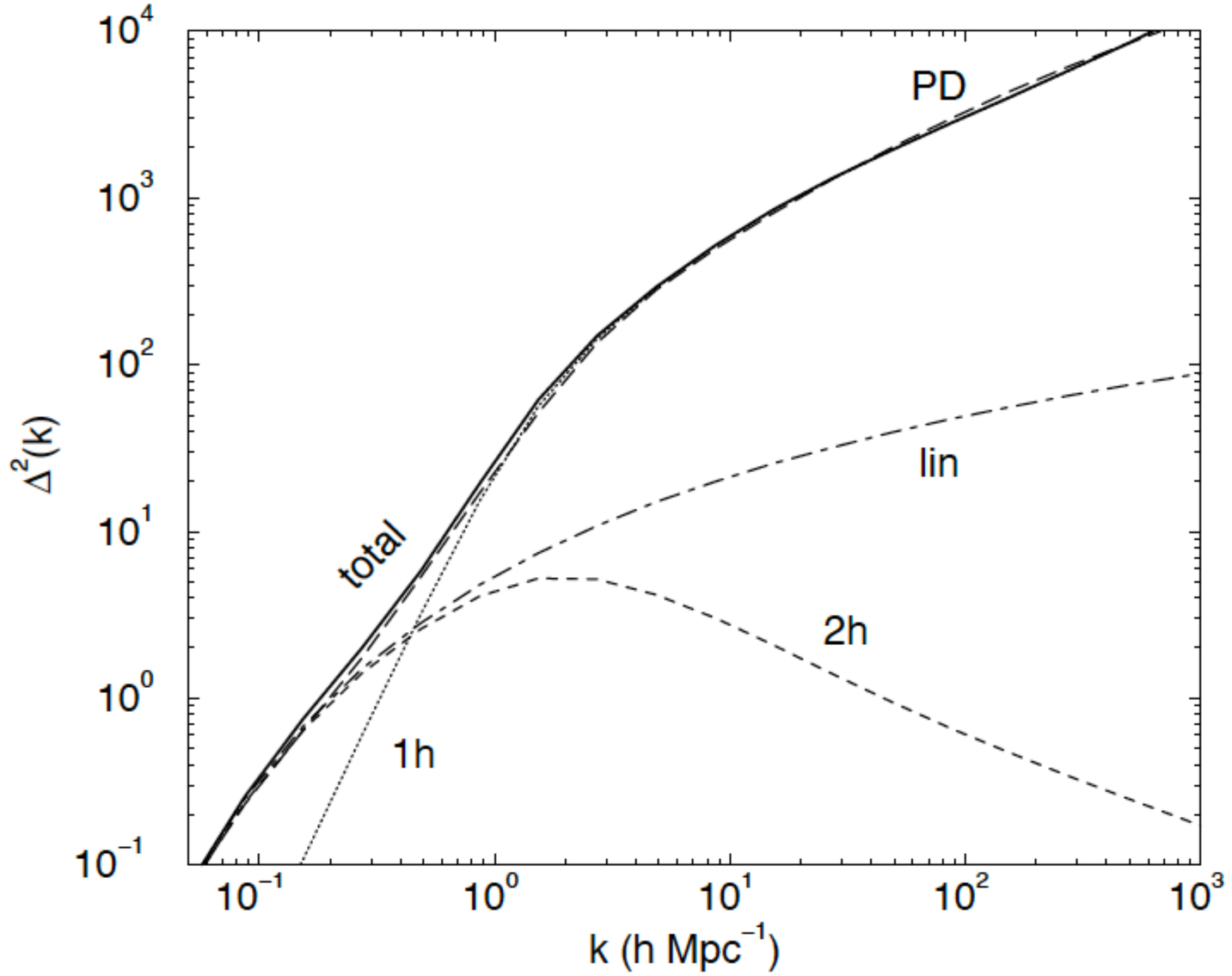

Cooray & Sheth 2002, Physics Reports, 372, 1

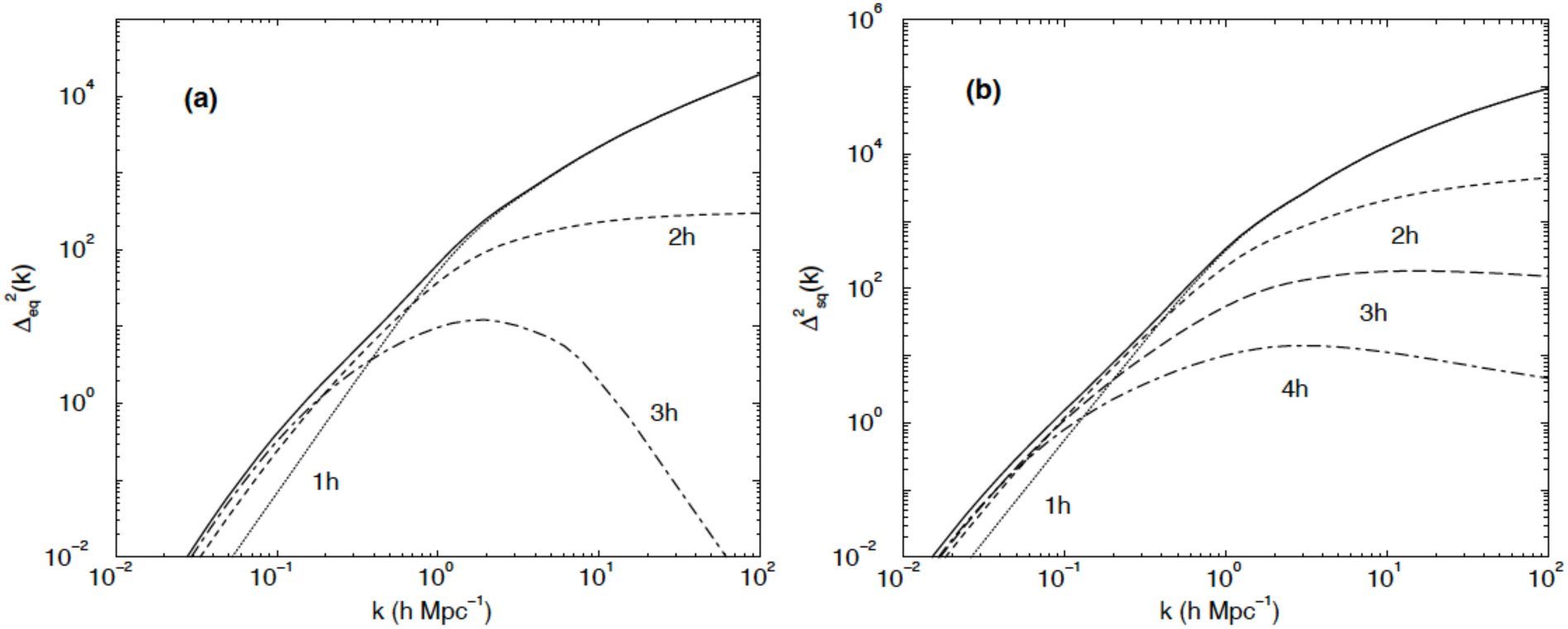

Cooray & Sheth 2002, Physics Reports, 372, 1

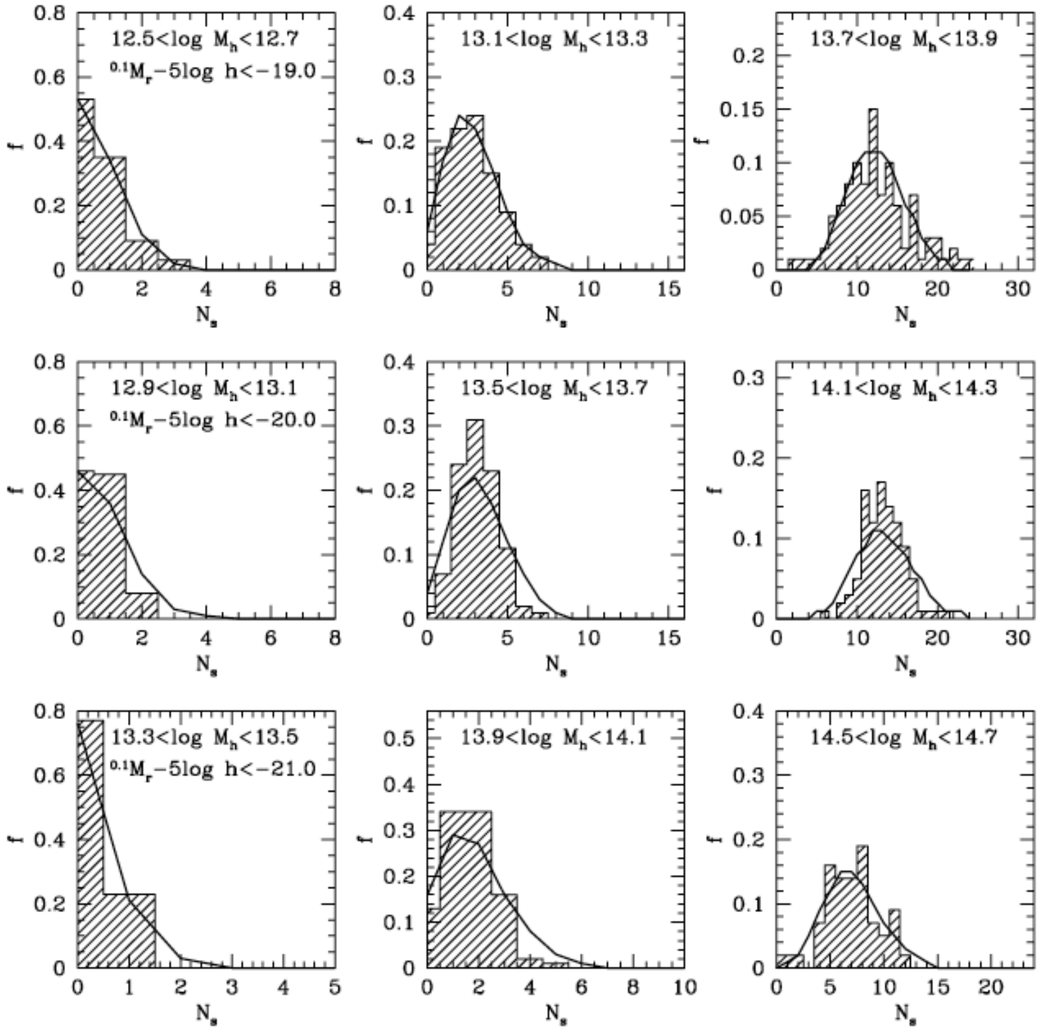

FIG. 10.— Number distributions of the satellite galaxies in groups of different halo mass bins, as indicated. The top, middle, and bottom rows correspond to different absolute magnitude limits as indicated. The hatched histograms indicate the distributions obtained from the groups in the SDSS. Thick solid curves correspond to Poisson distributions with the same mean N_s and are shown to illustrate the Poissonian nature of $P(N_s|M_h)$.

Yang et al. 2008, ApJ, 676, 248

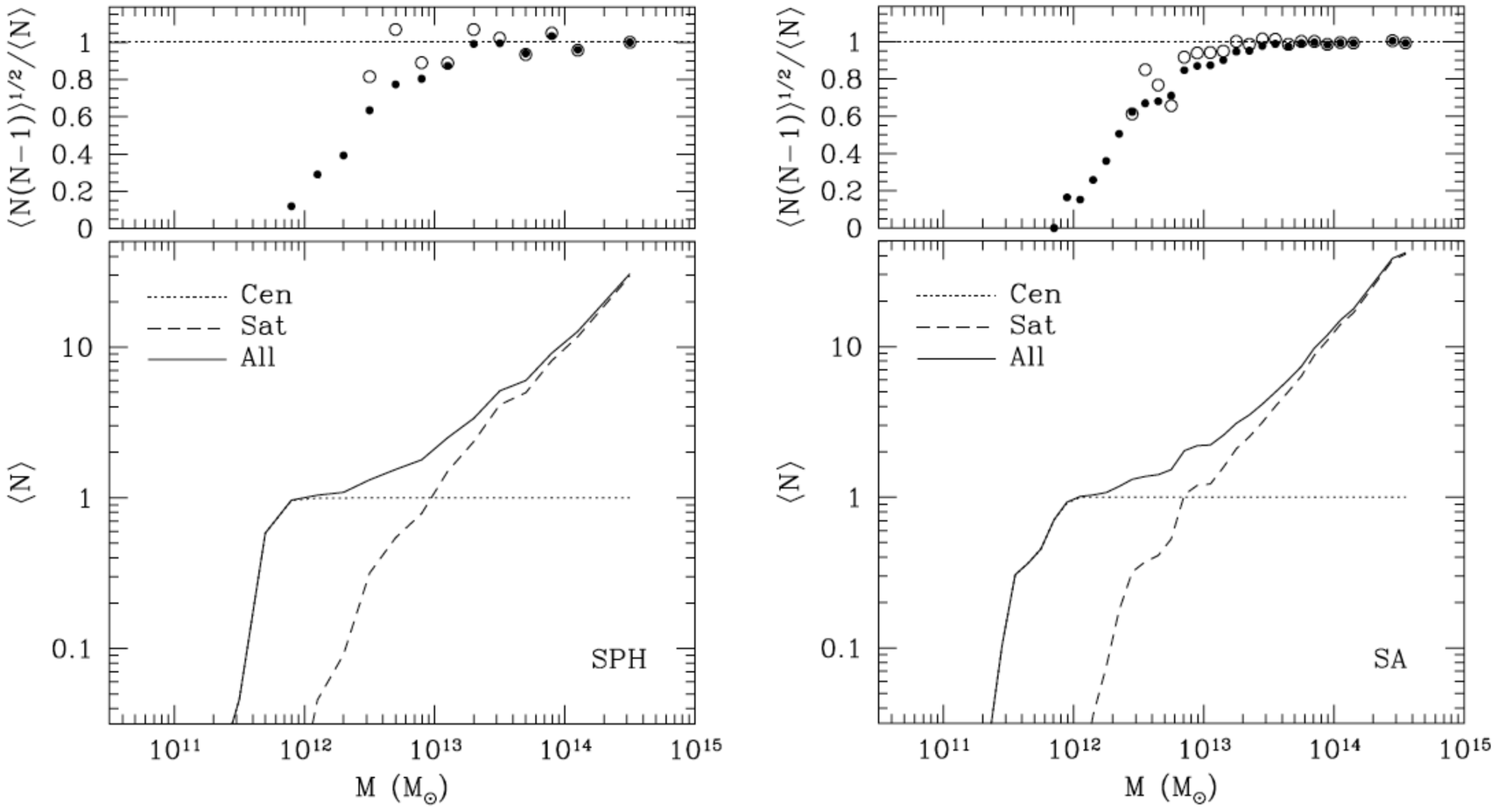

Zheng et al. 2005, ApJ, 633, 791

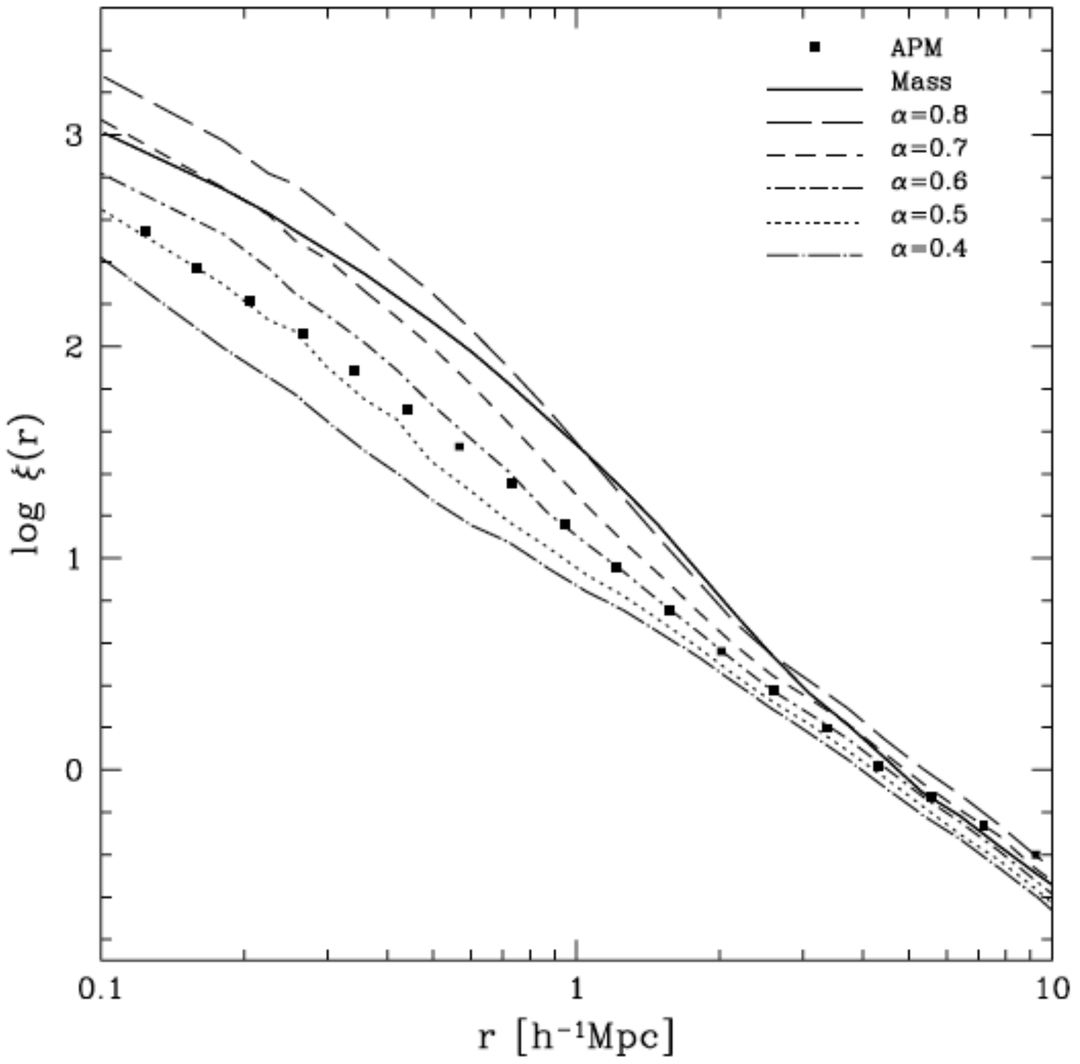

FIG. 4.—Influence of α on the galaxy correlation function. Curves show galaxy correlation functions for HOD models with a power-law $N_{\rm avg}(M)$, $M_{\rm min} = 2.8 \times 10^{11}\ h^{-1}\ M_{\odot}$, Average $P(N|N_{\rm avg})$, and different values of α, which are listed in the legend.

Berlind & Weinberg 2002, ApJ, 575, 587

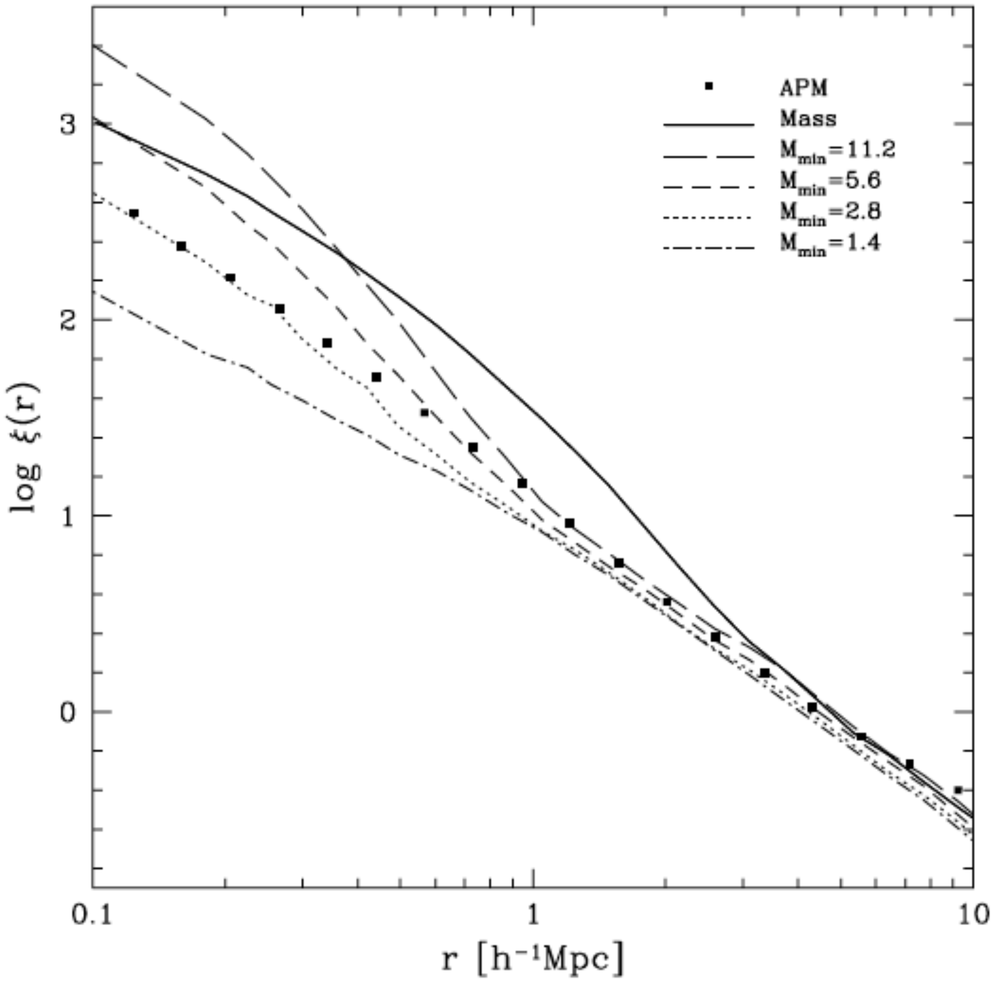

FIG. 3.—Influence of $M_{\rm min}$ on the galaxy correlation function. Curves show galaxy correlation functions for HOD models with a power-law $N_{\rm avg}(M)$, $\alpha = 0.5$, Average $P(N|N_{\rm avg})$, and different values of $M_{\rm min}$, which are listed in the legend in units of $10^{11}\ h^{-1}\ M\odot$. The solid curve shows the mass correlation function, and points show the correlation function measured from the APM galaxy survey (Baugh 1996).

Berlind & Weinberg 2002, ApJ, 575, 587

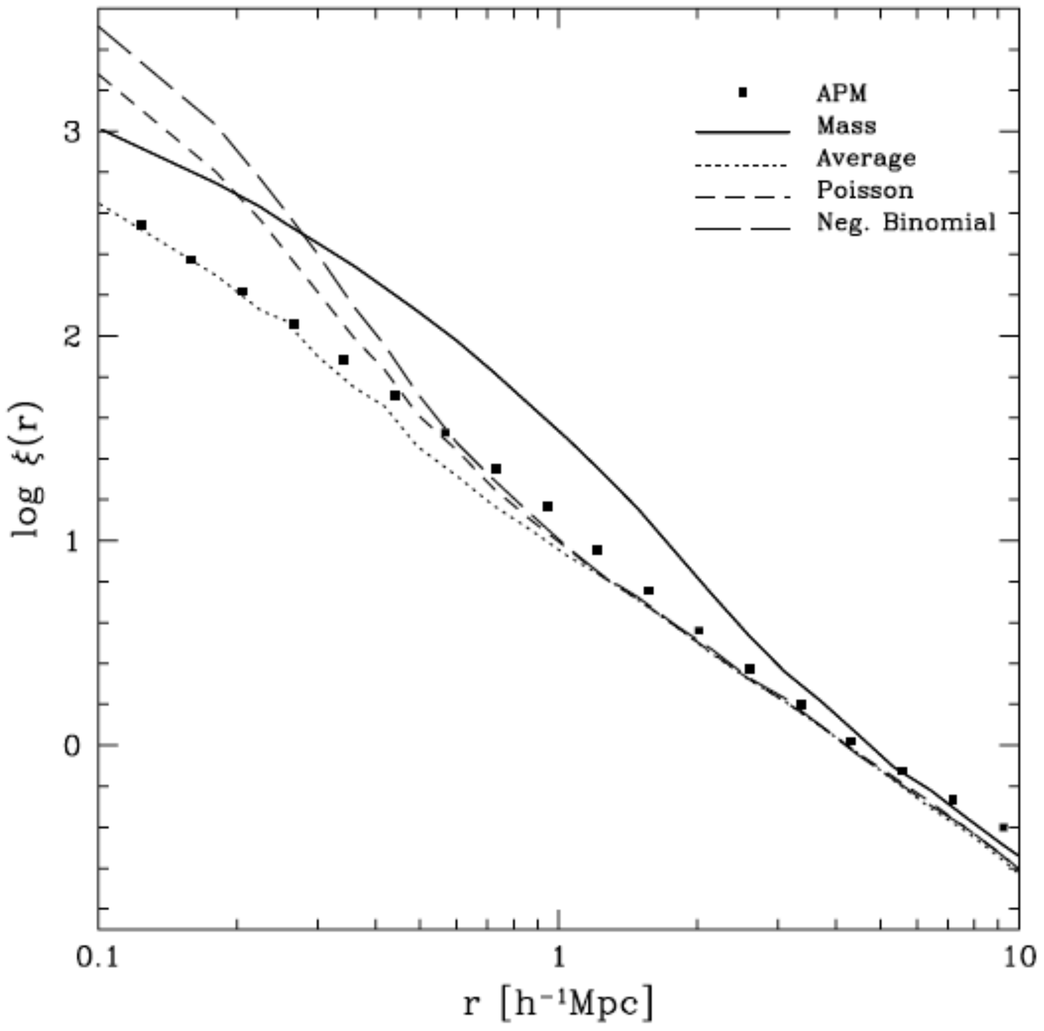

FIG. 5.—Influence of $P(N|N_{avg})$ on the galaxy correlation function. Curves show galaxy correlation functions for HOD models with a power-law $N_{avg}(M)$, $M_{min} = 2.8 \times 10^{11}\ h^{-1}\ M_{\odot}$, $\alpha = 0.5$, and different forms of $P(N|N_{avg})$, which are listed in the legend.

Berlind & Weinberg 2002, ApJ, 575, 587

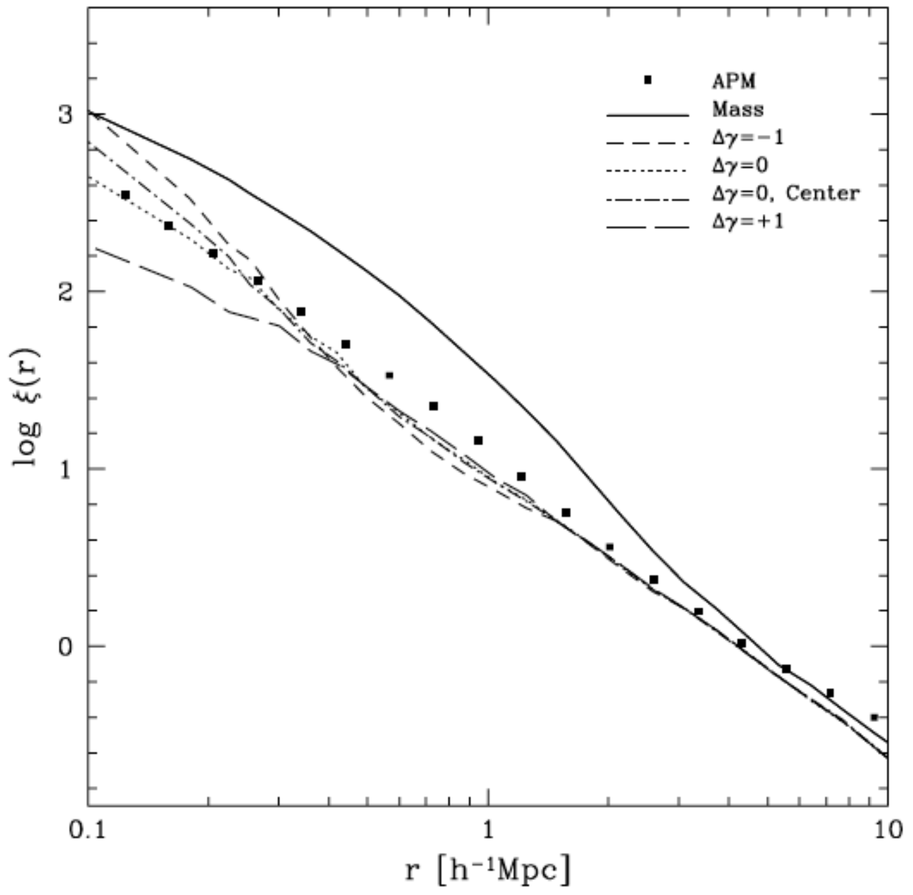

FIG. 6.—Influence of the galaxy profiles within halos on the galaxy correlation function. As in Figs. 3–5, the dotted curve shows $\xi_g(r)$ for a model with $M_{\rm min} = 2.8 \times 10^{11}\ h^{-1}\ M_\odot$, $\alpha = 0.5$, Average $P(N|N_{\rm avg})$, and galaxies tracing dark matter within halos. Short-dashed and long-dashed curves show results for models in which galaxy profiles are respectively more or less concentrated than dark matter profiles ($\Delta\gamma = -1$ or $\Delta\gamma = +1$; see eq. [3]). The dot-dashed curve shows a model in which the first galaxy of each halo lies at the halo center and subsequent galaxies have the same profile as the dark matter.

Berlind & Weinberg 2002, ApJ, 575, 587

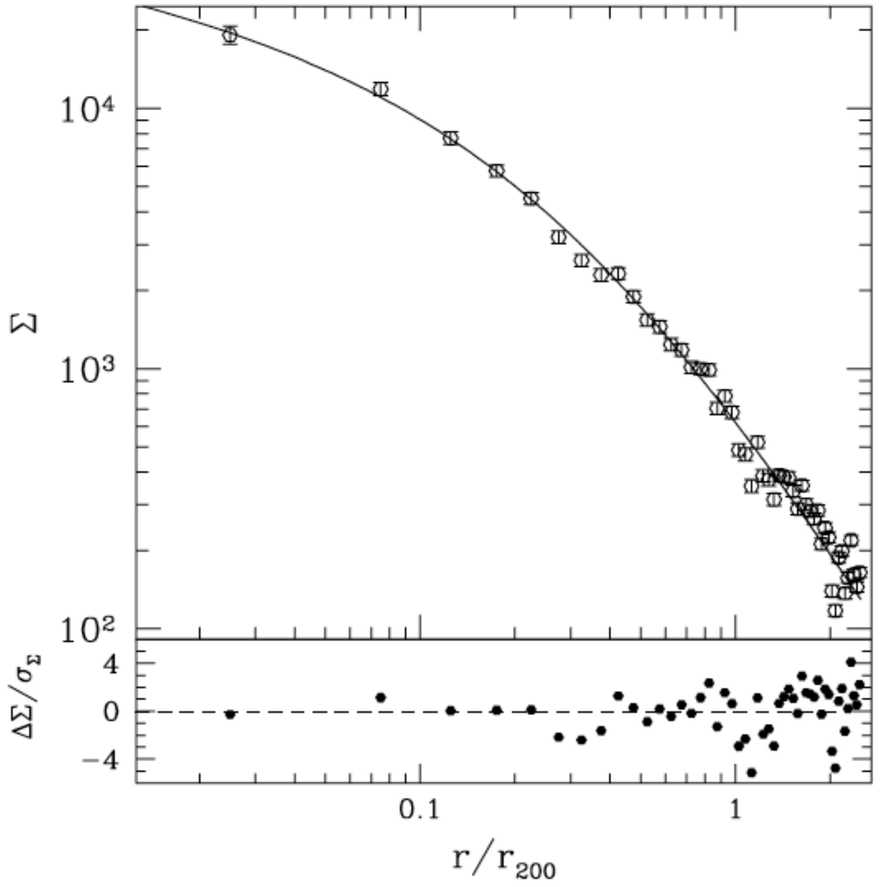

FIG. 1.—Composite galaxy surface density with BCGs excluded. The best-fit NFW profile is shown. The fit is obtained by fitting the data within r_{200} only. The figure shows the distribution of 6608 galaxies, of which 1467 (22%) are estimated to be background. *Bottom:* Residuals (differences between data and the fit) in units of standard deviation, which does not include the contribution from galaxy clustering.

Lin et al. 2004, ApJ, 610, 745

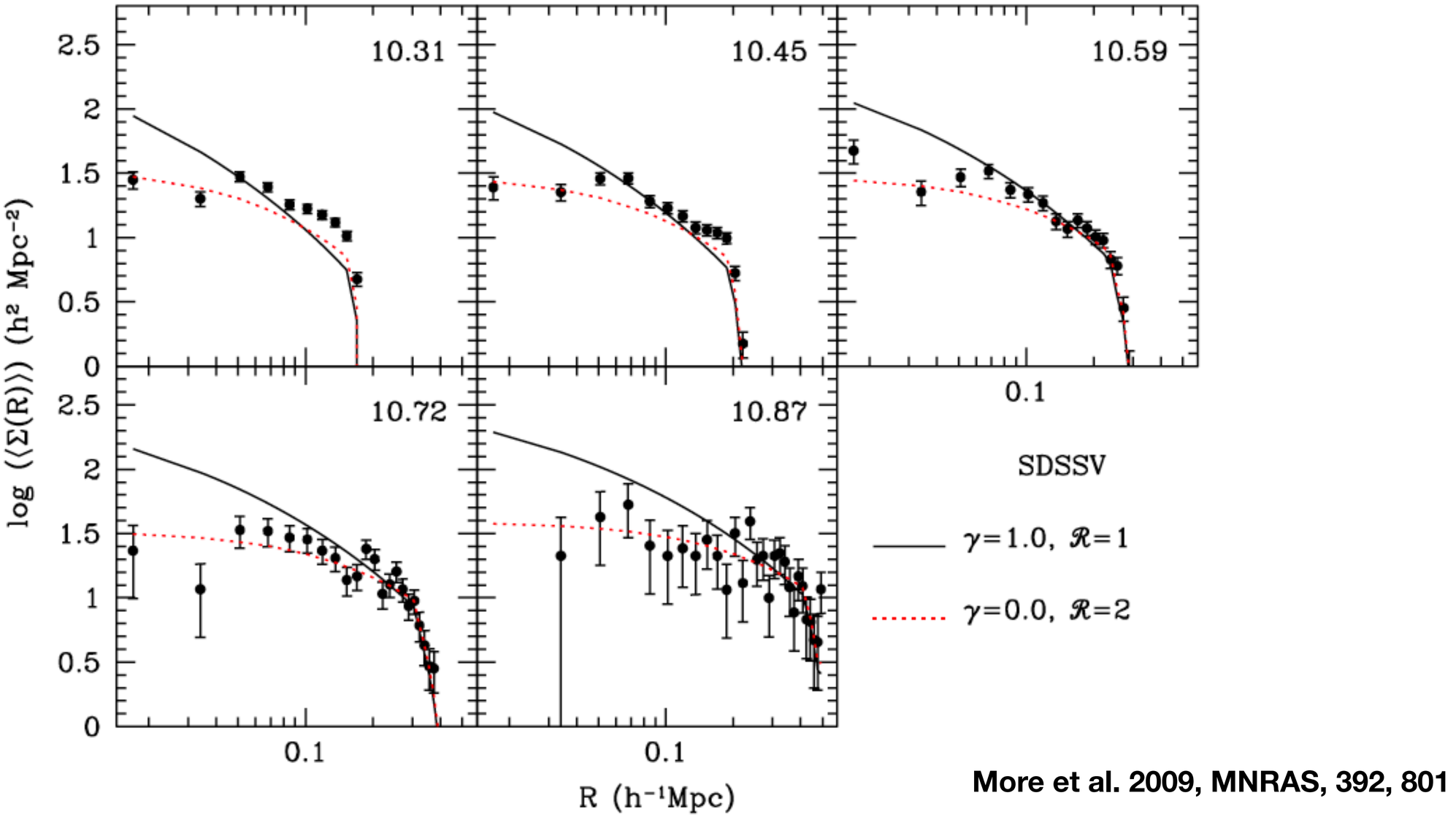

More et al. 2009, MNRAS, 392, 801

Zehavi et al. 2011, ApJ, 736, 59

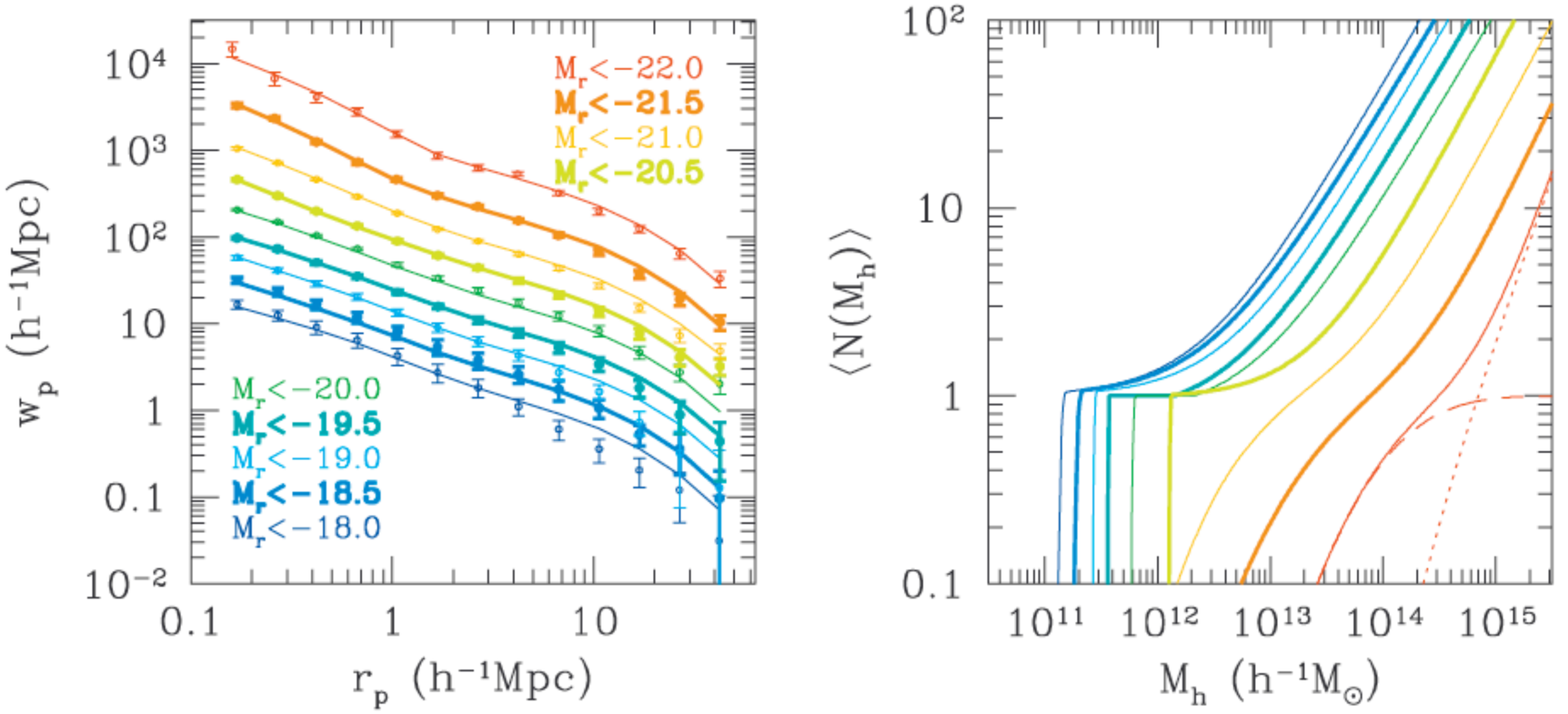

Figure 10. Luminosity dependence of galaxy clustering and the HOD. The left panel shows the measured $w_p(r_p)$ and the best-fit HOD models for all luminosity-threshold samples. The samples are each staggered by 0.25 dex, starting from the $M_r < -20.5$ sample, for clarity. The right panel shows the corresponding halo occupation functions, $\langle N(M_h)\rangle$, color-coded in the same way. The occupation functions shift to the right, toward more massive halos, as the luminosity threshold increases. The separation of central and satellite galaxies is shown for the rightmost occupation function, corresponding to the brightest sample, as the dashed and dotted curves, respectively. For the six fainter samples, we have chosen models with sharp central galaxy cutoffs ($\sigma_{\log M} \approx 0$) that have $\Delta\chi^2 < 1$ relative to the best-fit model listed in Table 3 (see the text). The three brightest samples *require* smooth cutoff profiles to fit the number density and clustering data.

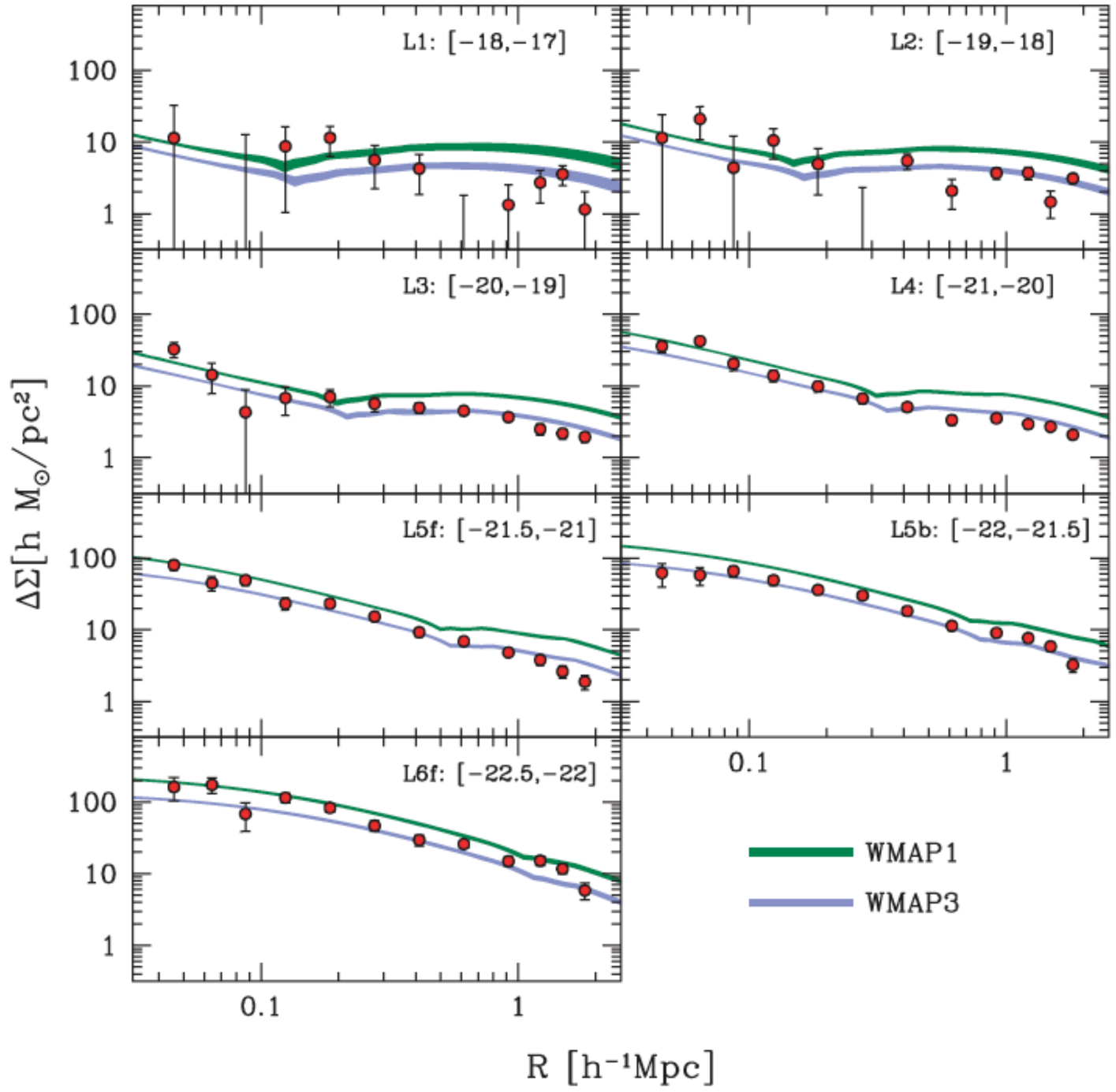

Cacciato et al. 2009, MNRAS, 394, 929

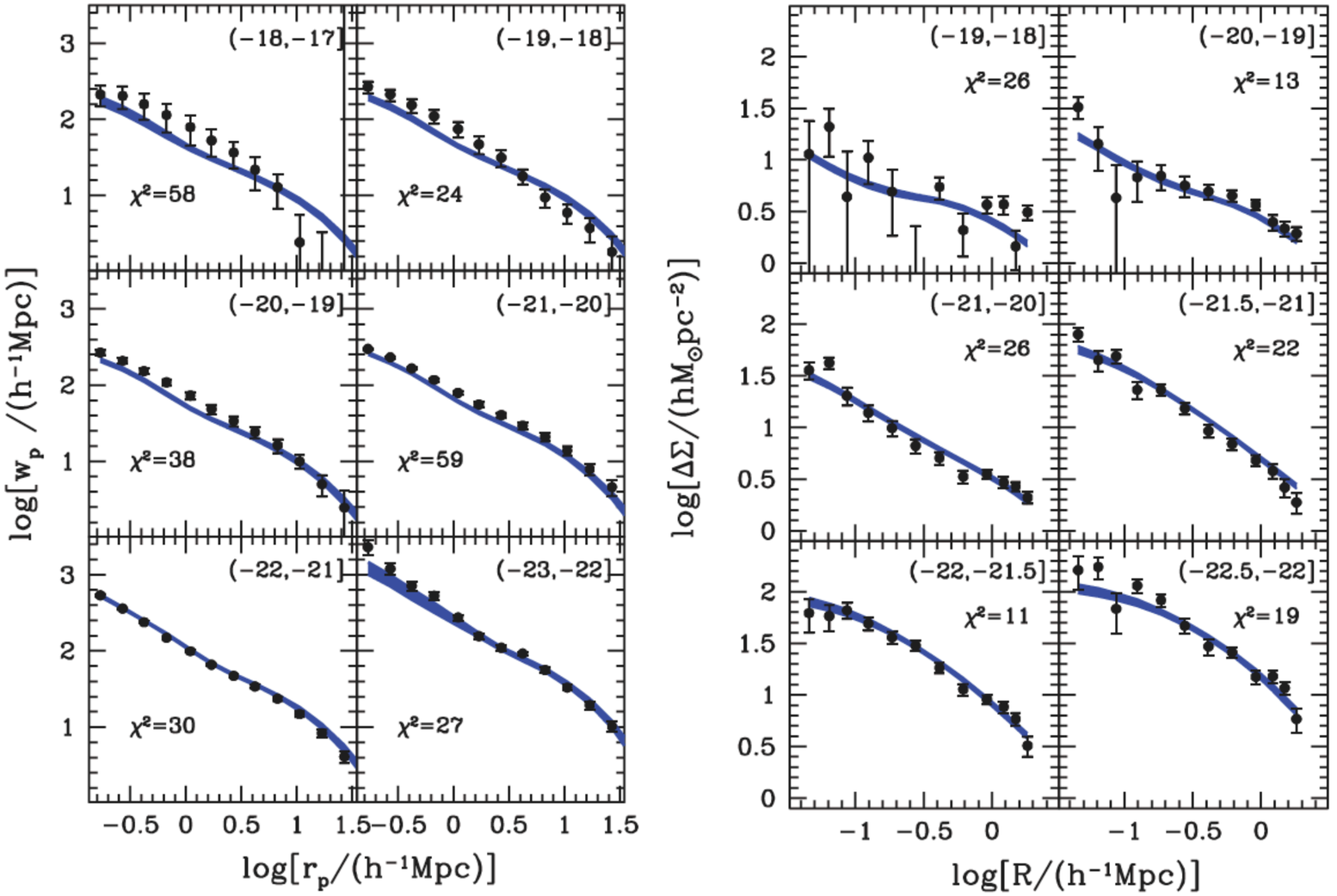

Cacciato et al. 2013, MNRAS, 430, 767

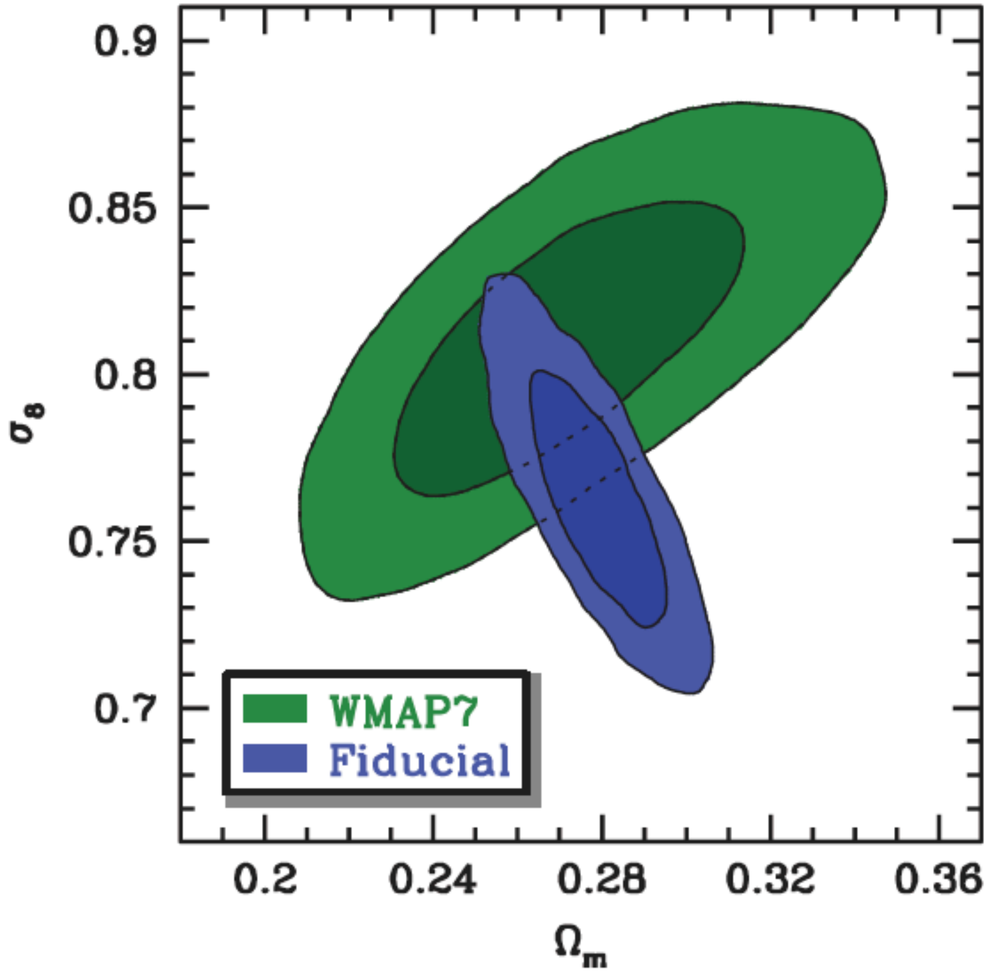

Figure 3. The 68 and 95 per cent CLs of the joint two-dimensional, marginalized posterior distribution for our `Fiducial` model, obtained from the simultaneous analysis of the abundance, clustering and lensing of galaxies in the SDSS. The green contours show the corresponding CLs for the *WMAP7* analysis of the CMB (Komatsu et al. 2011), and are shown for comparison.

Cacciato et al. 2013, MNRAS, 430, 767